ICONTECH INTERNATIONAL JOURNAL OF SURVEYS, ENGINEERING, TECHNOLOGY
ISSN 2717-7270
Journal homepage: http://icontechjournal.com/index.php/iij
Volume 6 (2022) Issue 4

A New Empirical Model for Thin-Layer Drying Modeling in the Stenter

Ram Makinesinde İnce Tabaka Kurutma Modelleme İçin Yeni Bir Ampirik Model

Ahmet Erhan Akan

Machinery and Metal Technology, Çorlu Vocational School, Tekirdağ Namık Kemal University, Çorlu, Tekirdağ, Türkiye

https://orcid.org/0000-0003-1806-7943

Corresponding author: aeakan@nku.edu.tr

ABSTRACT

This study involves the drying behaviour of a hot oil heated stenter used for drying and sizing of woven or knitted fabrics and modelling with a new empirical model developed. The suitability of the new model developed was compared with a theoretical model of First Order Kinetic model and 5 thin layer drying models selected from the literature. Statistical analyses between model and experimental data were evaluated by using MATLAB 2019a program as a benchmark. R^2 values in the regression analysis were taken as the main criterion. In addition, SEE and RMSE data were evaluated in determining model suitability. According to the results obtained, in the case that the drying behaviour of the stenter was modelled with a First Order Kinetic model, R^2 values between the model and experimental data were found to vary between 0.9933-0.9989. In the case of using 5 thin layer drying models selected from the literature, R^2 values were found to range between 0.9740 and 0.9999 and the most suitable model among them was Approximation of Diffusion model. R^2 values of the new empirical model developed were found to be between 0.9987 and 0.9999. Since the new model developed contains fewer model constants than other models available in the literature, it is concluding to provide practicality in researches on this subject and may display more sensitive results in determining thin layer drying behaviour.

Keywords: Drying, Ram machine, Stenter, Theoretical Modelling, Thin-layer modelling.

1. INTRODUCTION

Drying has been considered an important phenomenon used for different purposes since ancient times. The heat energy transferred to the material to be dried allows the moisture inside the material to be carried to the surface of the material and then removed from the material surface to the atmosphere [1-2]. Therefore, drying is a complex phenomenon involving simultaneous heat and mass transfer [3]. The main purpose of the drying processes is to perform the drying processes with minimum cost and maximum efficiency without compromising the quality of the products to be dried [4]. Drying processes are one of the most energy and time-consuming applications especially in textile production factories [5-6]. Thus, it is inevitable for the machines used in drying processes to be manufactured more efficiently. The machines heavily preferred in drying and thermosetting processes in the textile industry are stenters. Stenters are mainly used for two purposes. The first is to bring the moisture in the fabric to the desired rate (drying), and the other is to adjust the width of the fabric. Fabrics to be dried in stenters are fixed at the edges with needles or palettes. In this way, they are moved at the desired speed so

Received 1 November 2022; Received in revised form 18 December 2022; Accepted 20 December 2022; Available online 28 December 2022;
doi: 10.5281/zenodo.7489810

that they stay suspended in the stenter. Drying air is sent to the fabrics moving in the stenter, perpendicular to the fabric axis from below and/or above. Thus, with convective drying, the desired amount of dehumidification is achieved [7].

The textile materials used in this study are of hygroscopic and also porous materials. The moisture content of the hygroscopic materials varies according to the humidity of the air. As the humidity of the air increases, hygroscopic materials can retain more moisture [8]. Porosity is the case when the pore diameter of the material is equal to 10^{-7} m or greater than this value [5]. When the drying behaviour of porous hygroscopic fabrics dried in stenters is examined, the drying is observed to be in a decreasing speed period and the drying rate has a nonlinear relationship with time. In this respect, since the heat transfer coefficients change with the change of moisture content in the decreasing drying period, explaining the drying behaviour with the use of traditional heat transfer mechanisms will cause some errors. Thus, conventional heat transfer mechanisms can be used as modelling tools for a fixed drying period. In the decreasing drying period, non-linear modelling equations should be considered. Researchers have created a set of models based on diffusion theories and a number of boundary conditions to estimate the rate of moisture change under various boundary conditions. These models are models that are presented in differential form to describe the moisture content change in the fabric, based on the principle of chemical diffusion mechanism [9]. Moreover, in convective drying processes, diffusion theorem based on Fick's second law is often used to simulate mass transfer. But the exponential term in this theorem ($\exp(-\pi Dt^2/4L^2)$) causes some restrictions in decreasing drying period. For this, Efremow [10] proposed a mathematical solution to solve this problem by using error functions integrated into Fick's law. Kowalski et al. [11] used partial differential and numerical analysis methods to investigate the thermo-mechanical properties of the drying processes of porous materials. However, considering highly variable conditions in industrial drying processes, this method is not considered practical because it is a time-consuming application that requires extensive calculation [12].

When the thin-layer drying processes are examined in the literature, it can be seen that the materials to be dried are placed on the drying effect surface in a single layer and there are many experimental, semi-experimental and theoretical models trying to define the drying kinetics [13]. Mathematical models of thin-layer drying processes are extremely important in terms of improving the performance of drying systems, reducing energy efficiency and reducing emission values released to the environment [14]. However, there are a limited number of studies in the literature regarding the modelling of the drying kinetics of textile fabrics. When some of these studies are examined, Nordon and David [15] have found a finite difference solution based on the "double sweep" method to produce solutions to nonlinear differential equations that enable the combined diffusion of heat and mass (moisture) in hygroscopic textile materials. Besides, in addition to the diffusion equations, they developed a ratio equation where the rate of moisture exchange between solid (textile fibers) and gas phase (pore space) is tried to be explained. Luikov et al. [16] presented a method based on the relationship between Rebinder number and drying speed to calculate the drying kinetics occurring during the drying of damp materials in their studies. Blejchar et al. [17] performed mathematical modelling of water evaporation and drying air flow in a porous medium representing a fibrous material-cotton towel that was dried under real conditions. They used the finite volume method and the Euler multiple phase model in calculations. Johann et al. [18] tried to develop a model that simulates the drying times of dried textile materials. For this, they used the finite difference method in Cartesian coordinates. They used the Shapiro-Wilk test in order to examine the accuracy of the model and stated that the confidence level p value was greater than 5%,

Received 1 November 2022; Received in revised form 18 December 2022; Accepted 20 December 2022; Available online 28 December 2022;
doi: 10.5281/zenodo.7489810

indicating the accuracy of the model for all cases. Akan and Ünal [19], in their previous works that are different from this study, searched for the model that most accurately simulated thin layer drying behaviour in the ram machine using the empirical data of this study and 12 empirical models frequently used in the literature. Of the selected models, they concluded that the appropriate models were Diffusion approach, Two term, Modified Henderson and Pabis. As it can be understood from the literature research, although there are a limited number of studies examining the thin layer drying behaviour of textile materials, it is seen that this type of research is generally done on food drying processes. The most commonly used thin layer modelling tools for drying various materials in the literature and explanations showing the source of these studies are presented in Table 7 in the Modeling section.

In this study, the drying behaviour of a stenter used in the drying and sizing of knitted and woven fabrics in the production phase of a textile factory was modelled with a new empirical model developed, and the model fit was compared with the Theoretical model of First Order Kinetic model as well as 5 thin layer drying models selected from the literature. It is thought that the new model developed will define the thin layer drying kinetics quite appropriately and will show a practical approach to the employees with its four model constants, and it is a supportive study for the literature that is lacking in this regard.

2. MATERIALS AND METHOD

The experiments in this study were carried out in a textile factory under real production conditions in a 10-cabinet hot oil heated stenter (Fig. 1a-b) used in textile finishing processes. Thanks to the control unit (Figure 1c), each cabin of the stenter can be adjusted to a maximum drying temperature of 220 ºC, fabric speed of 5-100 m/min and fabric width of 60-240 cm. The thermal requirement of the stenter is provided by a natural gas oil boiler operating at 6 bar operating pressure with a capacity of $8x10^6$ kcal/h.

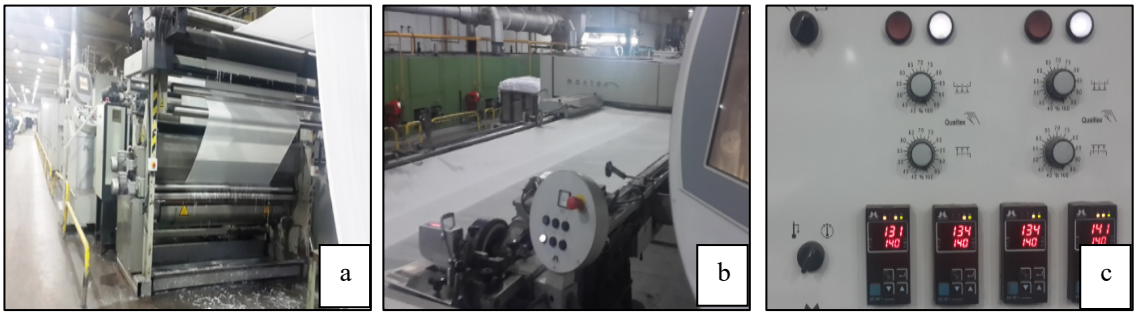

Figure 1 a- Fulard part, b- Fabric entrance to the cabinet, c- control unit Schematic representation of the stenter.

The schematic representation of the drying system is presented in Figure 2, and the schematic representation showing the location of the nozzles for each chamber and the measured locations are presented in Figure 3. In Figure 2, the hot oil from the hot oil boiler is brought to the desired temperature in the heat exchanger and sent to the nozzles in the dryer rooms (Figure 3) with the help of an automatic controlled fan. The part (control volume) examined in the study is shown with dashed lines, the items entering and leaving the control volume are numbered and a detailed representation of this part is given in Figure 3.

Received 1 November 2022; Received in revised form 18 December 2022; Accepted 20 December 2022;
Available online 28 December 2022;
doi: 10.5281/zenodo.7489810

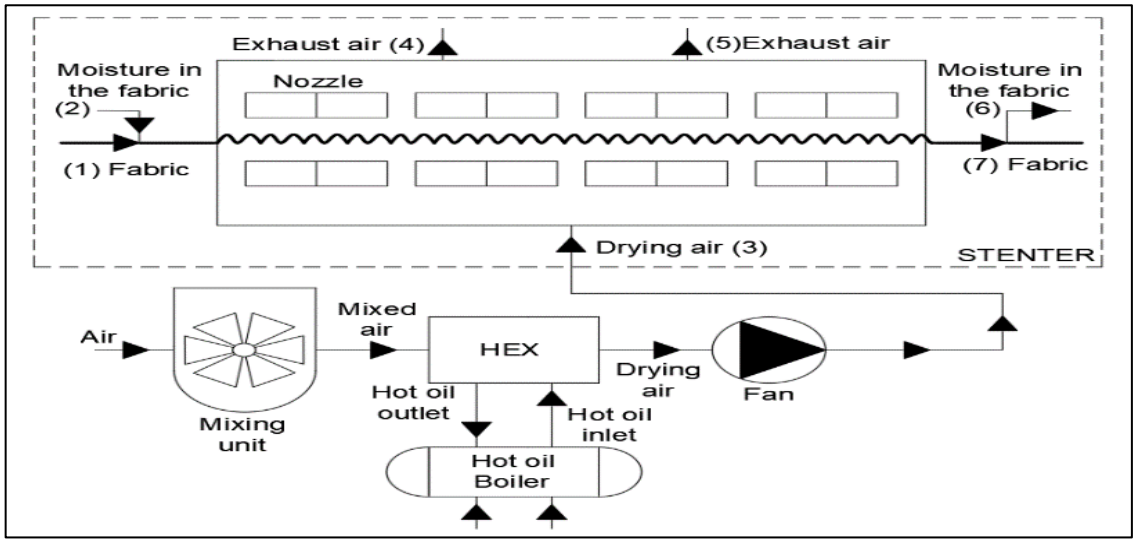

Figure 2. Schematic representation of the positions of the nozzles and measuring points

2.1. Experimental Procedure

In the experiments, Thessaloniki knitted fabrics with 67% cotton + 33% polyester content were used. In order to determine the dry weight of the fabric before drying, 5 samples of 100 cm^2 taken with DVT 100 sample cutter (±4% m^2) were kept in Electro-Mag M3025P drying oven (±1°C) for 24 hours at 65% [RH] relative humidity and 25 °C temperature. Dry weights of fabrics taken from the drying oven were determined as 320 g/m^2 using Neck Fly 300 precision scales (±0.001 g). The stenter consists of three parts which are fulard, dryer rooms (10 units) and cooling cabin. The fabrics which were taken to the wash process in the fulard part (Figure 1a) that enables the fabrics to be opened and purified from unwanted substances before drying, were subjected to pre-drying (mechanical drying) process on the rollers under a pressure of 5 bar in the same part. For this reason, for each drying operation, it was determined that the surface temperatures of the fabrics at the entrance of the dryer were 30 °C and relative humidity values were 80% [RH] using DHT-3 branded fabric surface moisture measuring device (±1%), and wet fabric weights were 576 g/m^2. Then, the experiments carried out in 9 different drying operations were repeated 3 times, with the fabrics taken into the drying cabinets (Figure 1b) at a feed rate of 9-12 and 15 m/min and at a drying temperature of 120-140 and 160 °C. Fabric surface temperatures were determined with K type thermocouples (± 1% °C) placed on the fabric and Testo 176 T4 branded data logger. To determine the evaporation amount, using the T/CK type probe (±1.5 - 3% [RH]) placed on the boundary layer between the fabric surface and drying air, the relative humidity of the waste air (air leaving the fabric surface) is detected with the help of Testo 635-1 branded hygrometer (Figure 3). The drying operation is completed when the dried fabrics pass through the cooler part that prevents excessive drying of the fabric at the exit of the stenter. In cases where the relative humidity of dried fabrics is around 5% [RH], the fabrics are considered to be dry.

Received 1 November 2022; Received in revised form 18 December 2022; Accepted 20 December 2022;
Available online 28 December 2022;
doi: 10.5281/zenodo.7489810

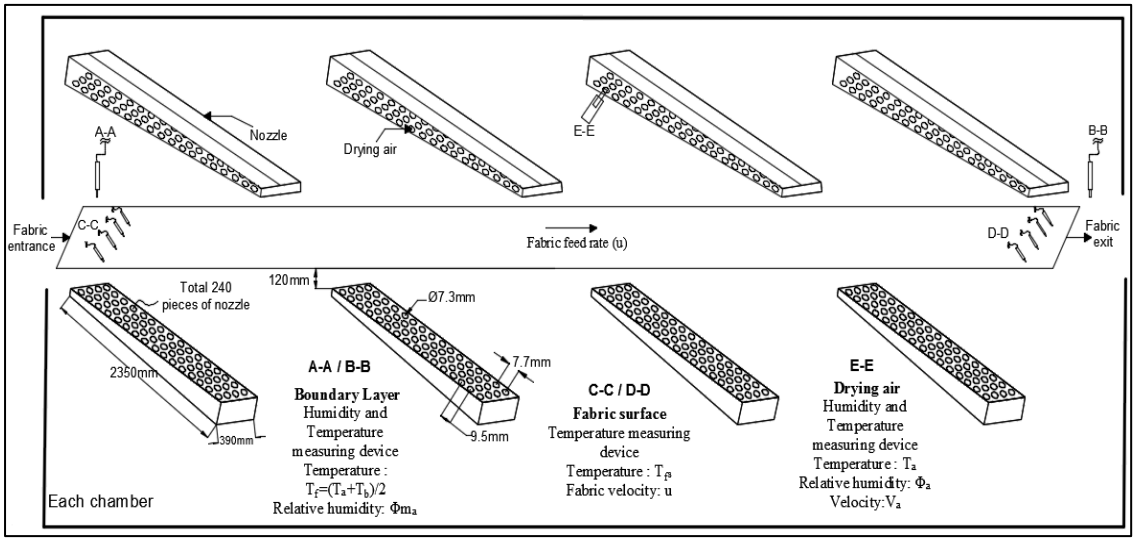

Figure 3. Location of nozzles and experimental measurement points

2.2. Data obtained from experiments

Since the fabrics taken to each room of the stenter have a total surface area of 3.6 m^2, with a width of 1.20 m and a length of 3 m, the damp weight (Mo) at the start of drying was determined as 2.073 kg and dry weight as 1.152 kg. At the time of the experiments, the ambient temperature was measured as 30 ºC and relative humidity as 65% [RH]. Moreover, depending on the operating conditions, the speed and flow rate of the air blown from the nozzles were measured with the Testo 440 dP brand gas analyzer device (±0.4%). Accordingly, measured air speeds and flow rates for drying air temperatures of 120-140 and 160 ºC were determined as 23.5-26.6-33.8 (m/s) and 0.199-0.233-0.275 (kg/s), respectively. The results are presented in Tables 1 and 2.

Table 1. FST values measured at the entry and exit points of each room of the dryer

Drying air temperature (ºC)	Fabric feed rate (m/s)	Fabric surface temperature each chamber (ºC)										
		Entrance	1st	2nd	3rd	4th	5th	6th	7th	8th	9th	10th
120	0.150	30	67	79	94	100	105	109	110	111	113	109
	0.200	30	67	76	80	86	93	95	107	111	112	108
	0.250	30	65	74	77	81	90	95	105	111	112	103
140	0.150	30	83	89	119	127	130	131	132	133	134	128
	0.200	30	76	87	91	105	116	121	125	129	133	128
	0.250	30	73	81	86	97	106	114	122	127	132	124
160	0.150	30	83	91	121	129	141	148	151	152	153	151
	0.200	30	82	88	93	102	134	141	148	151	152	144
	0.250	30	81	85	89	96	112	127	137	142	150	141

Received 1 November 2022; Received in revised form 18 December 2022; Accepted 20 December 2022;
Available online 28 December 2022;
doi: 10.5281/zenodo.7489810

In Table 1, when the fabric surface temperatures obtained from 9 different drying operations are examined, it can be seen that the fabric, which leaves the fulard part at 30 ºC, shows a rapid increase in surface temperature values in the first three cabinets and these temperature values approach the drying temperature after the 6th cabinet. Furthermore, temperature drops were seen in the 10th cabinets. The reason for this is thought to be the heat escaping from the fabric exit gap at the exit of the cabinet. Increasing the drying temperature causes an increase in the fabric surface temperature values. In the experiments, the highest fabric temperature was reached by obtaining a value of 153 ºC at the highest value of drying air (160 ºC) and the lowest value of the fabric speed (9m/min -0.150 m/s).

Table 2. Relative humidity values of damp air leaving the fabric surface, measured in the boundary layer

Drying air temperature (ºC)	Fabric feed rate (m/s)	Humidity of the circulating air Each chamber [%RH]									
		1st	2nd	3rd	4th	5th	6th	7th	8th	9th	10th
120	0.150	78.3	61.6	48.3	35.2	25.6	21.3	14.2	10.2	8.4	6.8
	0.200	72.4	57	44.5	32.8	24.1	20.6	13.9	9.9	8.2	6.4
	0.250	68.8	56.1	42.6	30.3	23.7	19.8	13.1	9.5	7.9	6.1
140	0.150	80.3	63	49	36.6	27.1	22.6	15.6	11.1	9	7.4
	0.200	74.2	58.3	45	34.5	22.5	21.8	14.9	10.3	8	6.2
	0.250	70.5	57.7	44.9	30.6	23.6	19.9	14.1	9.5	7.5	5.6
160	0.150	84	66.5	53.7	39	30.2	24	16.8	11.7	9.6	7.5
	0.200	79.2	60.1	46.8	35.6	27.9	22.4	16.2	11.5	9	6.3
	0.250	74.9	57.6	46.1	32.1	25.5	20.5	15.4	10.4	8.5	5.7

Table 2 presents the average relative humidity values taken from the hygrometer placed in the boundary layer formed between the fabric surface and drying air. From the relative humidity values, it is seen that drying takes place in the decreasing speed period. The decrease in the water in the fabric has started to make the drying process difficult. In this case, it can be understood from the decreasing humidity values that the drying occurs by diffusion. While the increase in fabric speed causes a decrease in humidity values, an increase in the drying temperature causes an increase in humidity values.

2.3 Analysis

The assumptions considered in the study are listed below.

1. The thermodynamic properties of the drying air blown from the dryer are constant.
2. Thermo-physical properties of the fabric are constant.
3. There is no moisture production and consumption within the fabric.
4. Moisture change in the fabric does not affect the drying temperature.
5. Dryer is adiabatic.
6. Moisture and temperature distribution in the fabric is constant.
7. Drying processes include simultaneous heat-mass transfer.
8. The amount of air blown into the cabinets is equal to the maximum amount of moisture that can be taken from the fabric.
9. It is assumed that the dried fabric is a rigid flat plate.

Received 1 November 2022; Received in revised form 18 December 2022; Accepted 20 December 2022; Available online 28 December 2022;
doi: 10.5281/zenodo.7489810

2.3.1 Determination of boundary layer thickness

During the drying process, in order to determine the boundary layer thickness between the drying air blown from the nozzles and the fabric surface dried, it was assumed that the maximum and minimum values of the fabric surface temperatures and the arithmetic mean of the drying air temperature values determined in the experiments were equal to the boundary layer temperature (Eq. 1) before starting the experiments where the data were taken. By accepting the fabrics as flat plates, kinematic viscosity (Eq. 2) and Reynolds numbers (Eq. 3) at the boundary layer temperature were determined. It is concluded that the flow is turbulent ($5x10^5 < Re < 10^7$) in the forced external convection on the fabrics accepted as flat plate in all operation conditions. Boundary layer thicknesses have been reached by using the 1/7th force law (Eq. 4) developed for turbulent flow in forced external convection on the flat layer with Reynolds numbers determined for operation conditions [20]. The results are presented in Table 3.

$$T_f = T_a + T_{fs} \tag{1}$$

In Equation 1, T_f is boundary layer (°C), T_a is drying air (°C), T_{fs} is fabric surface temperature(°C).

$$\nu = \frac{\mu}{\rho} \tag{2}$$

In this equation, υ is kinematic viscosity (m/s^2), μ is dynamic viscosity (kg/ms), ρ is density (kg/m^3).

$$Re = \frac{VL_c}{\nu} \tag{3}$$

In this equation, V is air speed (m/s), L_c is characteristic length (m), υ is kinematic viscosity (m/s^2).

$$\frac{\delta}{x} = \frac{0.16}{(Re_x)^{1/7}} \tag{4}$$

Here, δ is boundary layer thickness (m), x local layer length (m).

Table 3. Boundary layer thicknesses determined for all operating conditions**.**

Drying air temperature (°C)	Drying air speed (m/s)	Fabric surface temperature (°C)		Boundary layer temperature (°C)	Kinematic viscosity (m^2/s)	Reynolds number	Boundary layer thickness (mm)
		Min.	Max.				
120	**23.5**	65	-	92.5	22.34 x 10^{-6}	3155487	56.59
		-	113	116.5	22.92 x 10^{-6}	2828444	57.48
140	**26.6**	73	-	106.5	23.82 x 10^{-6}	3349461	56.11
		-	133	136.5	27.15 x 10^{-6}	2938708	57.17
160	**33.8**	81	-	120.5	25.37 x 10^{-6}	3996553	54.71
		-	153	156.5	29.49 x 10^{-6}	3438358	55.90

Received 1 November 2022; Received in revised form 18 December 2022; Accepted 20 December 2022;
Available online 28 December 2022;
doi: 10.5281/zenodo.7489810

Table 3 shows that the boundary layer thicknesses that will occur between the fabric surface and drying air vary between 55.9 and 57.48 mm in the experiments. Accordingly, it was determined that it would be appropriate to position the device to measure the relative humidity of the waste air (air leaving the fabric surface) 50-55 mm from the fabric surface during the experiments, and the experiments were carried out under these conditions.

2.3.2 Determination of the evaporation amount

The mass balance of the dryer is written according to the item numbers entering and leaving the control volume given in Figure 2.

Fabric $= \dot{m}_{f2} = \dot{m}_{f6} = \dot{m}_f$ (5)

Air $= \dot{m}_{a3} = \dot{m}_{a4} + \dot{m}_{a5} = \dot{m}_a$ (6)

Water $= \dot{m}_{w2} = \dot{m}_{w4} + \dot{m}_{w5} + \dot{m}_{w7} = \dot{m}_w$ (7)

In order to determine the amount of evaporation occurring in the drying rooms, it has been calculated according to the acceptance mentioned in the acceptance no. 8, "The amount of air blown into the cabinets is equal to the maximum amount of moisture that can be taken from the fabric". Accordingly, depending on the operating conditions, the flow rate of the air blown from the nozzles was determined and the evaporation amount was calculated by making use of the difference between the specific humidity of the humid air detected around the boundary layer and the specific humidity of the drying air (Eq.8).

$$M_e = 8x240\rho_{air}V_{air}A_{nozzle}(\omega_{moistair} - \omega_{dryair})t \quad (8)$$

Here, ρ is density of air (kg/m^3), V drying air speed (m/s), A nozzle area (m^2), ω specific humidity (g humidity/kg dry air), t (s) fabric retention time in the cabinet.

2.3.3 Determination of dimensionless humidity

The mathematical modelling of the drying processes takes into account the change in the moisture content of the product to be dried over time. It is known that especially when drying porous, hygroscopic and thin materials such as fabric, when the moisture contained in the product turns into water vapor, the resistance of this vapor against removal from the surface of the product is negligibly low. In this case, it is assumed that the drying rate depends on the diffusion in the material and the moisture content on the surface of the product is equal to the equilibrium moisture value (Me). This means that the moisture content on the surface is zero [21]. The expression that gives the dimensionless humidity used in mathematical models is presented in Equation 9 [22].

$$MR = \frac{M_t - M_e}{M_o - M_e} \quad (9)$$

In Equation 9, MR is dimensionless humidity, M_t is moisture content at any moment t (kg water/kg dry substance), M_o is initial moisture content (kg water/kg dry substance), M_e is balance moisture content (kg water/kg dry substance). Dimensionless moisture ratios obtained according to all operational conditions are presented in Table 4.

Received 1 November 2022; Received in revised form 18 December 2022; Accepted 20 December 2022;
Available online 28 December 2022;
doi: 10.5281/zenodo.7489810

Table 4. Dimensionless moisture values determined for all experiment conditions (MR).

Fabric feed rate (0.150 m/s)				Fabric feed rate (0200 m/s)				Fabric feed rate (0.250 m/s)			
Time (min)	**120 (ºC)**	**140 (ºC)**	**160 (ºC)**	**Time (min)**	**120 (ºC)**	**140 (ºC)**	**160 (ºC)**	**Time (min)**	**120 (ºC)**	**140 (ºC)**	**160 (ºC)**
0.000	1.000	1.000	1.000	**0.000**	1.000	1.000	1.000	**0.000**	1.000	1.000	1.000
0.333	0.739	0.725	0.718	**0.250**	0.758	0.755	0.734	**0.200**	0.770	0.776	0.739
0.667	0.573	0.556	0.530	**0.500**	0.580	0.593	0.549	**0.400**	0.619	0.623	0.556
1.000	0.440	0.414	0.387	**0.750**	0.446	0.450	0.417	**0.600**	0.482	0.486	0.420
1.333	0.330	0.295	0.289	**1.000**	0.347	0.344	0.315	**0.800**	0.402	0.387	0.341
1.667	0.242	0.216	0.213	**1.250**	0.288	0.272	0.241	**1.000**	0.343	0.320	0.274
2.000	0.184	0.159	0.161	**1.500**	0.242	0.220	0.190	**1.200**	0.298	0.270	0.225
2.333	0.151	0.122	0.127	**1.750**	0.200	0.185	0.155	**1.400**	0.260	0.234	0.189
2.667	0.125	0.100	0.098	**2.000**	0.170	0.154	0.124	**1.600**	0.228	0.201	0.157
3.000	0.104	0.079	0.074	**2.250**	0.149	0.128	0.098	**1.800**	0.202	0.171	0.128
3.333	0.092	0.067	0.055	**2.500**	0.132	0.103	0.076	**2.000**	0.184	0.141	0.104

2.4. Modelling

In the literature, there are three different modelling methods which are theoretical models derived from Fick's 2nd Law, semi-theoretical models created by theoretical and experimental studies, and experimental models. Thin layer modelling is generally used quite often in drying food products. 22 thin layer modelling methods used in the literature are given in Table 5. The new empirical model developed in this study was compared with the First Order Kinetic model, a theoretical model derived from Fick's second law, and 5 thin layer drying models frequently used in the literature. These 5 models examined are marked in Table 5 in bold color. The suitability of the models was determined by regression analysis investigated with the help of MATLAB R2019a program. For this, R^2, SEE, RMSE values were compared. R^2 values were chosen as the main criterion for determining model suitability. In the fit of the model, the closeness of the R^2 values to 1 and the closeness of SEE and RMSE values to 0 are the indicators of the fit of the model.

Table 5. Thin-layer models

No	Model name	Model	Reference
1	Newton model	$MR = \exp(-kt)$	23
2	Page model	$MR = \exp(-kt^n)$	24
3	Modified page (II)	$MR = \exp[-(Kt)^n]$	25
4	Modified page (III)	$MR = k \exp(-t/d^2)^n$	26
5	Henderson and Pabis model	$MR = a \exp(-kt^n)$	27
6	Modified Henderson and Pabis model	$MR = a \exp(-kt) + b \exp(-gt) + c \exp(-ht)$	28
7	Midilli and others model	$MR = a \exp(-kt) + bt$	29
8	Logarithmic model	$MR = a \exp(-kt) + c$	30
9	Two-term model	$MR = a \exp(-K_1t) + b \exp(-K_2t)$	31
10	Two-term exponential model	$MR = a \exp(-k_0t) + (1- a) \exp(-k_1at)$	32
11	Hii and others model	$MR = a \exp(-K_1t^n) + b \exp(-K_2t^n)$	33
12	Demir and others model	$MR = a \exp(-Kt)^n + b$	34
13	Verma and others model	$MR = a \exp(-kt) + (1-a) \exp(-gt)$	35
14	Approximation of diffusion	$MR = a \exp(-kt) + (1- a) \exp(-kbt)$	36
15	Modified Midilli and others	$MR = a \exp(-kt) + b$	37
16	Aghbashlo and others model	$MR = \exp[(K_1t)/(1+K_2t)]$	38
17	Wang and Singh	$MR = 1+at+bt^2$	39
18	Diamente and others model	$\ln(-\ln MR) = a +b(\ln t)+c(\ln t)^2$	40
19	Weibull model	$MR = \alpha - b \exp(-k_0 t^n)$	41
20	Thompson	$t = a \ln(MR) + b[\ln(MR)]^2$	42
21	Silva and others model	$MR = \exp(-at - b\sqrt{t})$	43
22	Peleg model	$MR = 1- t / (a+bt)$	44

Received 1 November 2022; Received in revised form 18 December 2022; Accepted 20 December 2022;
Available online 28 December 2022;
doi: 10.5281/zenodo.7489810

2.4.1 First Order Kinetic Model

First Order Kinetic model relates evaporation rate of water to moisture content [45]. The equation of the model is given in Equation 10.

$$-\frac{dM}{dt} = kM^{n} \tag{10}$$

In Equation 10, M is instant moisture content, n is degree constant, n = 1 for First Order Kinetic model. If the fabric moisture content is Mo at the beginning of the drying period, Equation 11 is obtained as a result of the integration of Equation 10 in the differential form.

$$\frac{M}{M_o} = e^{-kt} \tag{11}$$

Here k is kinetic coefficient. It is seen that instantaneous and initial moisture content ratios in the equation form an exponential relation with the kinetic coefficient k. When the natural logarithm is taken on both sides of the equation, this exponential relationship turns into a linear relationship and Eq. 12 is obtained.

$$ln\frac{M}{M_o} = -kt \tag{12}$$

In this case, ln(M/M0) – slope of the drying time (t) graph will give the kinetic coefficient k.

2.4.2 New model

When Table 5 is examined, it can be seen that exponential type or polynomial type functions are generally used as thin layer modelling tool. However, an experimental model has been developed in which the exponential and polynomial functions are evaluated together in order to model thin layer drying processes in the stenter due to the fact that these models can achieve more precise results or provide more practical use in terms of the number of model constants contained. For this, experimental data was used, and curve-settings program was used in MATLAB R2019a. The developed model is presented in Equation 13.

$$MR = a.exp(-bt) + ct^{2} + d \tag{13}$$

In this equation, refers to exponential type function, and the term refers to polynomial type function. In the equation, MR is dimensionless humidity, a, b, c and d are model constants (min^{-1}), t is drying time (min).

3. RESULTS AND DISCUSSION

The findings of the First Order Kinetic model to be used in the comparison of the new model and the 5 thin layer models selected from the literature are given below respectively. Also, equation 12 was used to determine the First Order Kinetic coefficient constant. The values obtained are shown in Table 12.

Received 1 November 2022; Received in revised form 18 December 2022; Accepted 20 December 2022;
Available online 28 December 2022;
doi: 10.5281/zenodo.7489810

Table 6. First Order Kinetic coefficient constants and R^2 analyses

Fabric feed rate (m/s)	Drying air temperature (°C)	Experimental kinetic coefficient k	Linear equation	Kinetic coefficient (R^2)	Experimental and Theoretical Model (R^2)
0,150 (9 m/min)	120	0.0123	y = -0.0123x-0.0892	0.9893	0.9977
	140	0.0139	y = -0.0139x-0.067	0.9933	0.9989
	160	0.0143	y = -0.0143x-0.0628	0.9984	0.9978
0,200 (12 m/min)	120	0.0135	y = -0.0135x-0.138	0.9830	0.9833
	140	0.015	y = -0.015x-0.0907	0.9932	0.9935
	160	0.0169	y = -0.0169x-0.0843	0.9965	0.9953
0,250 (15 m/min)	120	0.0139	y = -0.0139x-0.1459	0.9776	0.9947
	140	0.016	y = -0.016x-0.099	0.9906	0.9896
	160	0.0183	y = -0.0183x-0.125	0.9918	0.9865

When Table 6 is examined, it is seen that the kinetic coefficient increases with the increase in the fabric speed for the constant values of the drying temperature and the increase in the drying temperature at the same fabric speed. According to the assumptions made in all drying conditions, it was determined that the regression fit between the model and the experimental MR values would be between 0.9833 and 0.9989 in the case of using First Order Kinetic model to model the drying behaviour of the stenter. The results obtained for 5 thin layer models frequently used in the literature are given in Table 7.

Table 7. Statistical results of selected thin layer models

Model name: Newton						
FFR (m/s)	**DAT (°C)**	**Coefficients**		**SEE**	**RMSE**	**R^2**
		k				
0.150	**120**	0.8296		0.0019300	0.138900	0.9978
	140	0.8937		0.0010300	0.010150	0.9989
	160	0.9277		0.0011340	0.010650	0.9988
0.200	**120**	0.9792		0.0092200	0.030360	0.9884
	140	1.0210		0.0042020	0.020500	0.9950
	160	1.1350		0.0029650	0.017220	0.9966
0.250	**120**	1.0400		0.0179400	0.042360	0.9740
	140	1.1050		0.0063860	0.025270	0.9917
	160	1.2990		0.0093130	0.030520	0.9885
Model name: Henderson And Pabis						
FFR (m/s)	**DAT (°C)**	**Coefficients**		**SEE**	**RMSE**	**R^2**
		k	*a*			
0.150	**120**	0.8194	0.9887	0.0018130	0.014190	0.9977
	140	0.8900	0.9959	0.0010760	0.010940	0.9987
	160	0.8931	0.9638	0.0005756	0.007997	0.9930
0.200	**120**	0.9426	0.9669	0.0079150	0.029660	0.9889
	140	0.9957	0.9773	0.0038050	0.020560	0.9950
	160	1.0650	0.9412	0.0014640	0.012760	0.9981
0.250	**120**	0.9696	0.9440	0.0141800	0.039700	0.9771
	140	1.0690	0.9718	0.0051610	0.023950	0.9937
	160	1.2380	0.9572	0.0081230	0.030040	0.9889
Model name: Logarithmic						
FFR (m/s)	**DAT (°C)**	**Coefficients**			**SEE**	**RMSE**	**R^2**
		k	*a*	*c*			

Received 1 November 2022; Received in revised form 18 December 2022; Accepted 20 December 2022;
Available online 28 December 2022;
doi: 10.5281/zenodo.7489810

0.150	**120**	0.8958	0.9663	0.0325		0.0007618	0.009758	0.9989
	140	0.9320	0.9836	0.0169		0.0006711	0.009159	0.9991
	160	0.9720	0.9758	0.0204		0.0003090	0.006215	0.9996
0.200	**120**	1.2400	0.9056	0.0943		0.0001439	0.004240	0.9998
	140	1.1780	0.9381	0.0597		0.0005552	0.008331	0.9992
	160	1.2600	0.9525	0.0432		0.0002183	0.005223	0.9997
0.250	**120**	1.5020	0.8475	0.1486		0.0007970	0.009981	0.9986
	140	1.3740	0.9062	0.0932		0.0002471	0.005558	0.9996
	160	1.6020	0.9106	0.0837		0.0011140	0.011800	0.9983

Model name: Two Term

FFR (m/s)	DAT (°C)	Coefficients				SEE	RMSE	R^2
		k_o	k_1	a	b			
0.150	**120**	0.8434	-1.3980	0.9956	0.0003	0.0005260	0.008668	0.9992
	140	0.9017	-2.0720	0.9990	0.0000	0.0004337	0.007872	0.9993
	160	0.7806	1.5190	0.7112	0.2884	0.0002076	0.005445	0.9997
0.200	**120**	0.2102	1.3420	0.1738	0.8278	0.0000868	0.003521	0.9998
	140	1.2670	0.2808	0.8567	0.1424	0.0005432	0.008809	0.9991
	160	0.4786	1.4140	0.1892	0.8090	0.0001557	0.004716	0.9997
0.250	**120**	0.4191	2.0090	0.3965	0.6049	0.0004168	0.007716	0.9991
	140	1.5410	0.3522	0.7764	0.2247	0.0002125	0.005509	0.9996
	160	0.7848	2.4660	0.5098	0.4922	0.0004397	0.007926	0.9992

Model name: Approximation of Diffusion

FFR (m/s)	DAT (°C)	Coefficients			SEE	RMSE	R^2
		k	a	b			
0.150	**120**	0.8487	0.9995	-1.5030	0.0005610	0.008374	0.9992
	140	0.9029	1.0000	-2.2530	0.0004221	0.007264	0.9994
	160	1.5580	0.2697	0.5054	0.0002253	0.005306	0.9997
0.200	**120**	1.3370	0.8244	0.1617	0.0000690	0.002937	0.9999
	140	1.2760	0.8500	0.2315	0.0005443	0.008248	0.9992
	160	1.4260	0.8098	0.3324	0.0001270	0.003985	0.9998
0.250	**120**	2.2130	0.5489	0.2136	0.0002942	0.006064	0.9995
	140	1.5210	0.7888	0.2165	0.0002167	0.005204	0.9996
	160	2.4230	0.5004	0.3201	0.0004106	0.007164	0.9994

When the R^2 values obtained according to the models selected in Table 7 are examined, the R^2 values of the Newton model ranged between 0.9740 and 0.9989, and the R^2 values of the Henderson and Pabis model ranged between 0.9771 and 0.9989. Likewise, it can be seen that the R^2 values of the Logarithmic model ranged from 0.9983 to 0.9998, the R^2 values of the Two-Term model ranged from 0.9991 to 09998, and the R^2 values of the Approximation of Diffusion model ranged from 0.9992 to 0.9999.

The statistical results of the new model developed are given in Table 8.

Table 8. Statistical results of the new model developed

NEW MODEL

FFR (m/s)	DAT (°C)	Coefficients				SEE	RMSE	R^2
		a	b	c	d			
0.150	**120**	1.045	0.7904	0.005916	-0.0509	0.0004591	0.008099	0.9995
	140	1.069	0.8143	0.006586	-0.07305	0.0002998	0.006544	0.9997
	160	0.9349	1.051	-0.003699	0.06459	0.0001393	0.004461	0.9998
0.200	**120**	0.8809	1.302	-0.003763	0.1207	0.0000740	0.003251	0.9999
	140	0.9110	1.237	-0.003892	0.08842	0.0004577	0.008086	0.9995
	160	0.9281	1.320	-0.003755	0.0696	0.0001328	0.004345	0.9998
0.250	**120**	0.7798	1.741	-0.01623	0.2214	0.0003317	0.006884	0.9995
	140	-1.916	-0.5963	0.8853	2.911	0.0001333	0.004364	0.9998
	160	-2.02	-0.6502	1.125	3.008	0.0010140	0.102040	0.9987

Received 1 November 2022; Received in revised form 18 December 2022; Accepted 20 December 2022;
Available online 28 December 2022;
doi: 10.5281/zenodo.7489810

When the regression analysis results of the new model developed in Table 8 are examined, it can be seen that R^2 values vary between 0.9987 and 0.9999. In general, although R^2 values are quite high in all drying conditions, it is determined that this value decreases when the fabric speed and drying temperature are the highest. R^2 value was found to be 0.9987 for the case where drying temperature and fabric speed were the highest. However, this value shows that the model is quite suitable. As a result, it can be seen that the new model is quite suitable for thin layer drying modelling when compared with the first degree kinetic model and other selected models.

Instant dimensionless moisture ratios and instant moisture amounts obtained from experiments and new models of each drying operation are shown in Table 9-11.

Table 9. Model and experimental instant moisture amounts and instant dimensionless moisture ratios at 0.150 m/s fabric speed.

Fabric feed rate (0.150 m/s)												
	120 (°C)				140 (°C)				160 (°C)			
Time (min)	**Exp. MR**	**Mod. MR**	**Exp. m***	**Mod. m***	**Exp. MR**	**Mod. MR**	**Exp. m***	**Mod. m***	**Exp. MR**	**Mod. MR**	**Exp. m***	**Mod. m***
0.000	1.000	0.994	0.921	0.916	1.000	0.996	0.921	0.917	1.000	1.000	0.921	0.921
0.333	0.739	0.753	0.681	0.693	0.725	0.743	0.668	0.684	0.718	0.723	0.661	0.666
0.667	0.573	0.569	0.528	0.524	0.556	0.551	0.512	0.508	0.530	0.527	0.488	0.486
1.000	0.440	0.430	0.405	0.396	0.414	0.407	0.381	0.375	0.387	0.388	0.356	0.357
1.333	0.330	0.324	0.304	0.299	0.295	0.300	0.272	0.276	0.289	0.289	0.266	0.266
1.667	0.242	0.246	0.223	0.226	0.216	0.221	0.199	0.203	0.213	0.217	0.196	0.200
2.000	0.184	0.188	0.170	0.173	0.159	0.163	0.146	0.150	0.161	0.164	0.148	0.151
2.333	0.151	0.147	0.139	0.135	0.122	0.123	0.112	0.113	0.127	0.125	0.117	0.115
2.667	0.125	0.118	0.115	0.109	0.100	0.096	0.092	0.088	0.098	0.095	0.090	0.088
3.000	0.104	0.100	0.096	0.092	0.079	0.079	0.073	0.073	0.074	0.071	0.069	0.066
3.333	0.092	0.090	0.085	0.083	0.067	0.071	0.062	0.065	0.055	0.052	0.051	0.048

Table 10. Model and experimental instant moisture amounts and instant dimensionless moisture ratios at 0.200 m/s fabric speed

Fabric feed rate (0.200 m/s)												
	120 (°C)				140 (°C)				160 (°C)			
Time (min)	**Exp. MR**	**Mod. MR**	**Exp. m***	**Mod. m***	**Exp. MR**	**Mod. MR**	**Exp. m***	**Mod. m***	**Exp. MR**	**Mod. MR**	**Exp. m***	**Mod. m***
0.000	1.000	1.002	0.921	0.923	1.000	0.999	0.921	0.921	1.000	0.998	0.921	0.919
0.250	0.758	0.757	0.698	0.697	0.755	0.757	0.695	0.697	0.734	0.737	0.676	0.678
0.500	0.580	0.579	0.534	0.533	0.593	0.578	0.546	0.533	0.549	0.548	0.506	0.505
0.750	0.446	0.450	0.411	0.415	0.450	0.447	0.414	0.411	0.417	0.412	0.384	0.380
1.000	0.347	0.357	0.320	0.328	0.344	0.349	0.317	0.321	0.315	0.314	0.290	0.289
1.250	0.288	0.288	0.265	0.265	0.272	0.276	0.250	0.255	0.241	0.242	0.222	0.223
1.500	0.242	0.237	0.223	0.218	0.220	0.222	0.203	0.205	0.190	0.189	0.175	0.174
1.750	0.200	0.199	0.184	0.184	0.185	0.181	0.171	0.167	0.155	0.150	0.143	0.138
2.000	0.170	0.171	0.157	0.157	0.154	0.150	0.142	0.138	0.124	0.121	0.114	0.111
2.250	0.149	0.149	0.137	0.137	0.128	0.125	0.118	0.115	0.098	0.098	0.090	0.090
2.500	0.132	0.131	0.122	0.121	0.103	0.105	0.094	0.097	0.076	0.080	0.070	0.074

Received 1 November 2022; Received in revised form 18 December 2022; Accepted 20 December 2022;
Available online 28 December 2022;
doi: 10.5281/zenodo.7489810

Table 11. Model and experimental instantant moisture amounts and instant dimensionless moisture ratios at 0.250 m/s fabric speed

Fabric feed rate (0.250 m/s)												
	120 (°C)				140 (°C)				160 (°C)			
Time (min)	Exp. MR	Mod. MR	Exp. m*	Mod. m*	Exp. MR	Mod. MR	Exp. m*	Mod. m*	Exp. MR	Mod. MR	Exp. m*	Mod. m*
0.000	1.000	1.001	0.921	0.922	1.000	0.995	0.921	0.916	1.000	0.988	0.921	0.910
0.200	0.770	0.771	0.709	0.710	0.776	0.788	0.715	0.726	0.739	0.753	0.681	0.693
0.400	0.619	0.607	0.570	0.559	0.623	0.621	0.574	0.572	0.556	0.568	0.512	0.523
0.600	0.482	0.490	0.444	0.451	0.486	0.490	0.448	0.451	0.420	0.429	0.387	0.395
0.800	0.402	0.405	0.370	0.373	0.387	0.390	0.357	0.360	0.341	0.330	0.314	0.304
1.000	0.343	0.342	0.316	0.315	0.320	0.318	0.294	0.293	0.274	0.263	0.252	0.242
1.200	0.298	0.295	0.274	0.271	0.270	0.267	0.249	0.246	0.225	0.220	0.208	0.203
1.400	0.260	0.258	0.239	0.237	0.234	0.231	0.215	0.213	0.189	0.193	0.174	0.178
1.600	0.228	0.228	0.210	0.210	0.201	0.203	0.185	0.187	0.157	0.171	0.145	0.158
1.800	0.202	0.203	0.186	0.187	0.171	0.175	0.157	0.161	0.128	0.142	0.118	0.131
2.000	0.184	0.181	0.169	0.166	0.141	0.138	0.130	0.127	0.104	0.093	0.096	0.086

The harmony shown by the new model and experimental instant dimensionless moisture ratios are given in Figure 4-6, respectively.

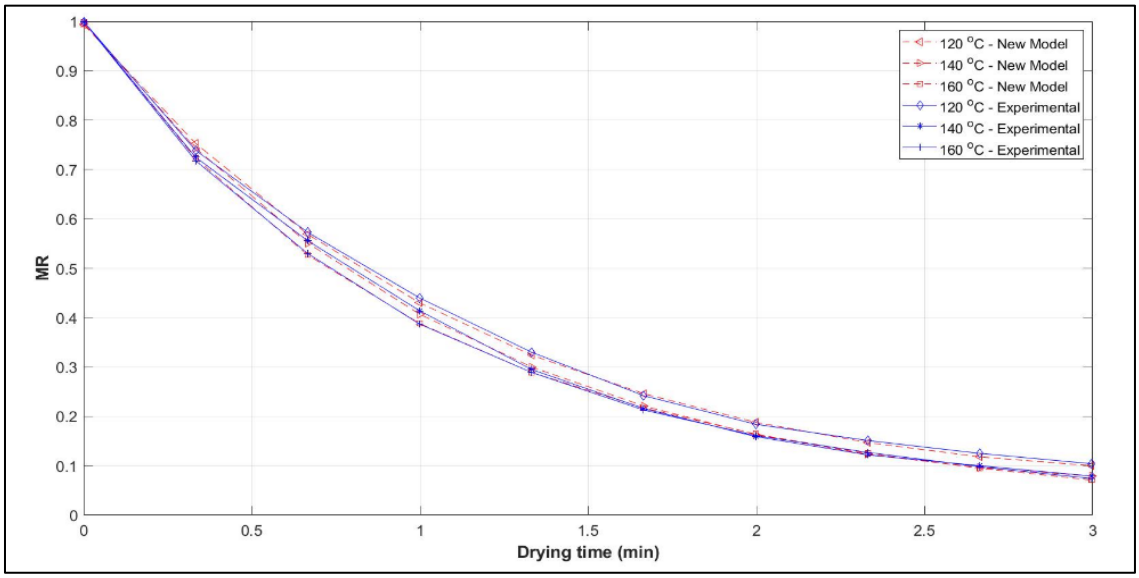

Figure 4. Change of MR values of experimental and new model in 0.150 (m/s) FFR over time.

Received 1 November 2022; Received in revised form 18 December 2022; Accepted 20 December 2022;
Available online 28 December 2022;
doi: 10.5281/zenodo.7489810

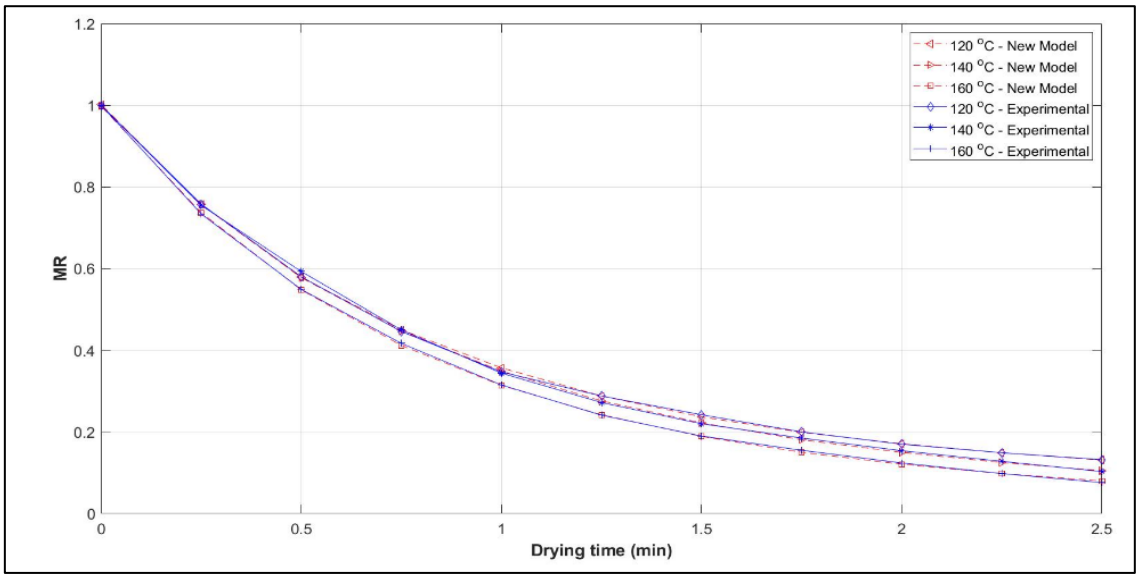

Figure 5. Change of MR values of experimental and new model in 0.200 (m/s) FFR over time.

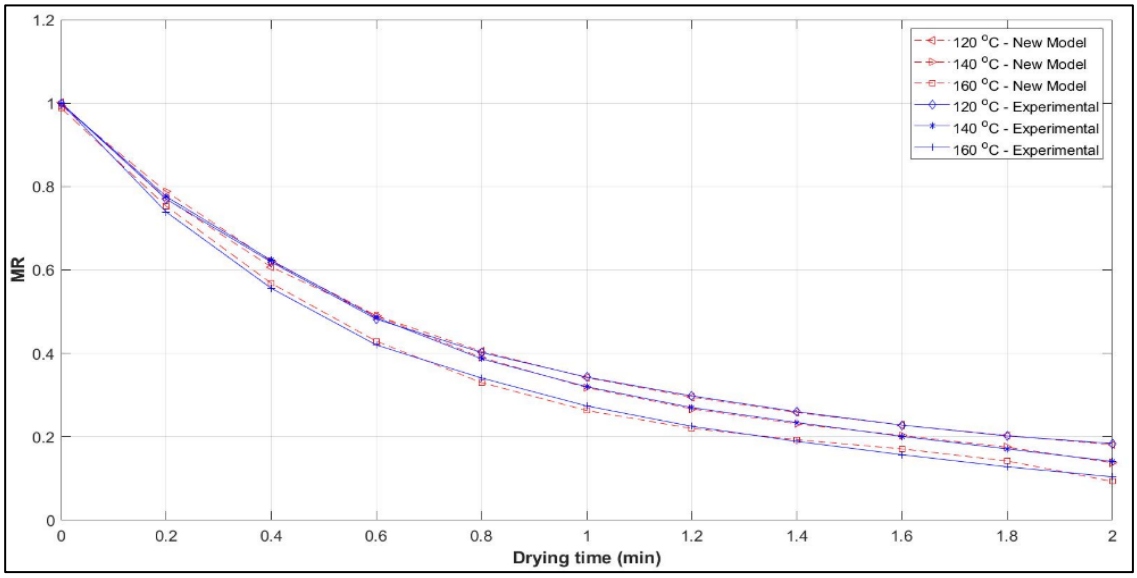

Figure 6. Change of MR values of experimental and new model in 0.250 (m/s) FFR over time.

When Figure 4-6 is analysed, it is seen that the new model developed with experimental MR values shows great harmony.

4. CONCLUSIONS

The findings obtained in this study are presented below as items.

1. It was observed that the surface temperature of the fabric that came out from the fulard part at 30 ° C and entered the dryer at this temperature in all operating conditions, increased rapidly in the first three cabinets, and after the 6th cabinet, it was seen that the fabric temperature approached the drying temperature.

Received 1 November 2022; Received in revised form 18 December 2022; Accepted 20 December 2022;
Available online 28 December 2022;
doi: 10.5281/zenodo.7489810

2. The highest fabric temperature was determined as 153 ºC in the operating condition where the drying air temperature was the highest (160 ºC) and the fabric advance rate was the lowest (0.150 m/s).

3. With the evaluation of data obtained from the waste air moisture leaving the fabric surface, it was determined that the drying process carried out in the stenter was in the rate of decreasing humidity. In addition, it was determined that the drying started with diffusion after the 6th Cabinet.

4. In the case that the First Order Kinetic model, which is a theoretical model, is used in the modelling of the drying process, it has been determined that the R^2 values are between 0.9833 and 0.9989 according to the statistical analysis performed for each drying operation.

5. In the case that the drying phenomenon occurring in the stenter is modelled with 5 thin layer models selected from the literature, it was determined that the statistical R^2 values of the models varied between 0.9740 and 0.9999. It was determined that the model that showed the best fit among these models was the Approximation of Diffusion model and R^2 values varied between 0.9992 and 0.9999.

6. R^2 values for all operation conditions of the new type model developed were found to vary between 0.9987 and 0.9999. Moreover, R^2 values were found to be 0.9995 and above in all drying operations except drying conditions (R^2 = 0.9987) where the drying air temperature was 160 ºC and the fabric speed was 0.250 m/s.

From the results obtained, it was concluded that the new type model developed was suitable to be used as a thin layer drying model in stenters. Furthermore, researching that this model can also be used as a food drying modelling tool, it is thought that it will display a more practical way compared to the use of models with more coefficients and constants.

Abbreviations

FFR Fabric feed rate

DAT Drying air temperature

Exp. Experimental

Mod. Model

REFERENCES

1. Ekechukwu, O.V. Review Of Solar-Energy Drying Systems I: An Overview Of Drying Principles And Theory. Ener. Conver. Manage. 1999, 40(6), 593–613. DOI: 10.1016/S0196-8904(98)00092-2

2. Akpinar, E.K., Bicer, Y. Modeling Of The Drying Of Eggplants In Thin-Layers. Int. J. Food Sci. Technol. 2005, 40, 273–81. DOI: 10.1111/j.1365-2621.2004.00886.x

3. Cengel, Y.A.; Ghajar A.J. Heat and Mass Transfer: Principles and Applications; Fourth Edition, New York, McGraw-Hill, 2015.

4. Oktay, Z.; Hepbasli, A. Performance Evaluation of a Heat Pump Assisted Mechanical Opener Dryer. Ener. Conver. and Manage. 2003, 44, 1193–1207. DOI: 10.1016/S0196-8904(02)00140-1

Received 1 November 2022; Received in revised form 18 December 2022; Accepted 20 December 2022; Available online 28 December 2022;
doi: 10.5281/zenodo.7489810

5. Mujumdar, A.S., "Handbook of Industrial Drying", Marcel, D., Ed. Inc. New York and Basel, 1995. pp. 948, 1987.6- Kudra T. 2004. Energy aspects in drying. Drying Technology 22(5):917–932.

7. Çay, A.; Tarakçıoğlu, I.; Hepbaşlı, A. Exergetic Performance Assessment of a Stenter System in a Textile Finishing Mill, Int. J. Energy Res. 2007, 31, 1251-1265. DOI: 10.1002/er.1295

8. Karakoca, A. Determination of the Temperature Area in Yarn Bobbin Drying Process by Finite Difference Method, Msc Thesis, Namık Kemal University Institute of Science, Tekirdağ, Turkey, 2017.

9. Ip, R.W.L.; Wan, I.C. New Use Heat Transfer Theories for the Design of Heat Setting Machines for Precise Post-Treatment of Dyed Fabrics. J. Defect and Diffusion Forum, 2011, 312-315, 748-751. DOI:10.4028/www.scientific.net/DDF.312-315.748

10. Efremov, G.I. Drying Kinetics Derived from Diffusion Equation with Flux-Type Boundary Conditions. Drying Technol. 2002, 20(1), 55-66. DOI: 10.1081/DRT-120001366

11. Kowalski, S.J.; Musielak, G.; Banaszak, J. Experimental Validation of the Heat and Mass Transfer Model for Convective Drying. Drying Technol. 2007, 25(1-3), 107-121. DOI: 10.1080/07373930601160940

12. Khazaei, J.; Chegini, G.R.; Bakhshiani, M. A Novel Alternative Method for Modeling the Effects of Air Temperature and Slice Thickness on Quality and Drying Kinetics of Tomato Slices: Superposition Technique. Drying Technol. 2008, 26(6), 759-775. DOI: 10.1080/07373930802046427

13. Özdemir, M. and Y.O., Devres, 1999. The Thin Layer Drying Characteristics of Hazelnuts during Roasting. Journal of Food Engineering, 42; 225-233.

14. Cihan, A., Kahveci, K. and O., Hacıhafızoğlu, 2007. Modelling of Intermittent Drying of Thin Layer Rough Rice. Journal of Food Engineering, 79; 293-298.

15. Nordon, P., David, H.G., 1967. Coupled diffusion of moisture and heat in hygroscopic textile materials. International Journal of Heat and Mass Transfer, 10(7); 853-866.

16. Luikov, A.V., Sheiman, V.A., Kuts, P.S., Slobodkin, L.S., 1967. An approximate method of calculating the kinetics of the drying process, Journal of engineering physics, 13; 387–393.

17. Blejchar, T., Raska, J., Jablonska, J., Mathematical Simulation of Drying Process of Fibrous Material, EPJ Web of Conferences 180, 02010 (2018), https://doi.org/10.1051/epjconf/201818002010.

18. Johann, G., E. A. Silva, E.A., Motta Lima, O.C., Pereira, N.C., 2014. Mathematical Modeling of a Convective Textile Drying Process, Brazilian Journal of Chemical Engineering, 31(4); 959-965.

19. Akan, A.E, Ünal, F., (2020). Thin-Layer Drying Modeling in the Hot Oil-Heated Stenter, International Journal of Thermophysics, 41;114, https://doi.org/10.1007/s10765-020-02692-x.

20. Akan, A.E.; Özkan, D.B.; (2019). Experimental examination and theoretical modeling of drying behavior in the ram machine, Drying Technology, https://doi.org/10.1080/07373937.2019.1662436.

21. Geankoplis, C.j. Transport Processes and Separation Process Principles, Fourth Edition, Prentice Hall, 2003.

Received 1 November 2022; Received in revised form 18 December 2022; Accepted 20 December 2022; Available online 28 December 2022;
doi: 10.5281/zenodo.7489810

22. Karathanos, V.T. Determination of Water Content of Dried Fruits by Drying Kinetics. J. Food Eng. 1999, 39, 337-344. DOI: 10.1016/s0260-8774(98)00132-0

23. El-Beltagy, A.; Gamea, G.R.; Essa, A.H.A. Solar Drying Characteristics of Strawberry. J Food Eng. 2007, 78, 456–64. DOI:10.1016/j.jfoodeng.2005.10.015

24. Akoy, E.O. Experimental Characterization and Modeling of Thin-Layer Drying of Mango Slices. Int. Food Res. J. 2014, 21(5), 1911–7.

25. Vega, A.; Fito, P.; Andr´es, A.; Lemus, R. Mathematical Modeling of Hot-Air Drying Kinetics of Red Bell Pepper (var. Lamuyo). J Food Eng. 2007, 79, 1460–6. DOI: 10.1016/j.jfoodeng.2006.04.028.

26. Kumar, P.D.G.; Hebber, U.H.; Ramesh M.N. Suitability of Thin Layer Models for Infrared-Hot-Air Drying of Onion Slices. LWT-Food Sci. Technol. 2006, 39(6), 700–5.

27. Meisami-asl E, Rafiee S, Keyhani A, Tabatabaeefar A. 2010. Determination of suitable thin-layer drying curve model for apple slices (Golab). Plant OMICS 3(3):103–8.

28. Zenoozian, M.S.; Feng, H.; Shahidi, F.; Pourreza, H.R. Image analysis and dynamic modeling of thin-layer drying of osmotically dehydrated pumpkin. J Food Process Preserv. 2008, 32, 88–102. https://doi.org/10.1111/j.1745-4549.2007.00167.x

29. Darvishi H, Hazbavi E. 2012. Mathematical modeling of thin-layer drying behavior of date palm. Glob J Sci Front Res Math Dec Sci 12(10):9–17.

30. Rayaguru K, Routray W. 2012. Mathematical modeling of thin-layer drying kinetics of stone apple slices. Intl Food Res J 19(4):1503–10.

31. Sacilik K. 2007. Effect of drying methods on thin-layer drying characteristics of hull-less seed pumpkin (Cucurbita pepo L.). J Food Engr 79(1):23–30. doi:10.1016/j.jfoodeng.2006.01.023

32. Dash KK, Gope S, Sethi A, Doloi M. 2013. Star fruit slices. Intl J Agric Food Sci Technol 4(7):679–86.

33. Kumar N, Sarkar BC, Sharma HK. 2012b. Mathematical modeling of thin-layer hot air drying of carrot pomace. J Food Sci Technol 49(1):33–41.doi:10.1007/s13197-011-0266-7

34. Demir VA˜ , Gunhan T, Yagcioglu AK. 2007. Mathematical modeling of convection drying of green table olives. Biosyst Engr 98:47–53. doi:10.1016/j.biosystemseng.2007.06.011

35. Akpinar, E.K. Determination of Suitable Thin-Layer Drying Curve Model for Some Vegetables and Fruits. J. Food Engr. 2006a, 73, 75–84. doi:10.1016/j.jfoodeng.2005.01.007

36. Yaldız, O.; Ertekin, C. Thin-layer Solar Drying of Some Vegetables. Drying Technol. 2007, 19(3-4), 583–97. DOI: 10.1081/DRT-100103936

37. Gan, P.L.; Poh, P.E. Investigation on the Effect of Shapes on the Drying Kinetics and Sensory Evaluation Study of Dried Jackfruit. Int. J. Sci. Engr. 2014, 7, 193–8. DOI: 10.12777/ijse.7.2.193-198

38. Aghbashlo, M.; Kianmehr, M.H.; Khani, S.; Ghasemi, M. Mathematical Modeling of Thin-Layer Drying of Carrot. Int. Agrophys. 2009, 23, 313-7.

Received 1 November 2022; Received in revised form 18 December 2022; Accepted 20 December 2022; Available online 28 December 2022;
doi: 10.5281/zenodo.7489810

39. Omolola, A.O.; Jideani, A.I.O.; Kapila, P.F. Modeling Microwave-Drying Kinetics and Moisture Diffusivity of Mabonde Banana Variety. Int. J. Agric. Biol. Engr. 2014, 7(6), 107–13. DOI:10.3965/j.ijabe.20140706.013

40. Diamante L, Durand M, Savage G, Vanhanen L. 2010a. Effect of temperature on the drying characteristics, colour and ascorbic acid content of green and gold kiwifruits. Intl Food Res J 451:441–51.

41. Tzempelikos DA, Vouros AP, Bardakas AV, Filios AE, Margaris DP. 2015. Experimental study on convective drying of quince slices and evaluation of thin-layer drying models. Engr Agric Environ Food 8(3):169–77.

42. Pardeshi IL, Arora S, Borker PA. 2009. Thin-layer drying of green peas and selection of a suitable thin-layer drying model. Drying Technol 27(2):288–95. doi:10.1080/07373930802606451

43. Pereira W, Silva CMDPS, Gama FJA. 2014. Mathematical models to describe thin-layer drying and to determine drying rate of whole bananas. J Saudi Soc Agric Sci 13(1):67–74. doi:10.1016/j.jssas.2013.01.003

44. Da Silva WP, Rodrigues AF, Silva CMDPS, De Castro DS, Gomes JP. 2015. Comparison between continuous and intermittent drying of whole bananas using empirical and diffusion models to describe the processes. J Food Engr 166:230–6. doi:10.1016/j.jfoodeng.2015.06.018

45. Ip, R.W.L and Wan, E.I.C., The new use of diffusion theories for the design of heat setting process in fabric drying, Advances in Modeling of Fluid Dynamics, Chapter 7, Intech, (2012), DOI:10.5772/48484.

Received 1 November 2022; Received in revised form 18 December 2022; Accepted 20 December 2022; Available online 28 December 2022;
doi: 10.5281/zenodo.7489810